Thin ZIF-8 Nanosheets Synthesized in Hydrophilic TRAPs

SCHOLARONE™
Manuscripts

PAPER

Thin ZIF-8 Nanosheets Synthesized in Hydrophilic TRAPs

Koki Sasaki, Tsuyoshi Okue, Yasuhiro Shu, Koji Miyake, Yoshiaki Uchida* and Norikazu Nishiyama

The preparation method of nanosheets using the hyperswollen lyotropic lamellar phases, 'two-dimensional reactors in amphiphilic phases (TRAP) method,' has successfully given nanosheets of various non-layered materials. Previously reported examples started from a single hydrophobic or hydrophilic precursor and multiple hydrophobic precursors. Here we propose the synthesis method of nanosheets of ZIF-8, zinc 2-methylimidazolate with a sodalite-like framework. They grow up to a few nanometers of thickness and several hundred nanometers of width with neither aggregation nor impurities from multiple hydrophilic precursors with the stoichiometric ratio inside the hydrophilic TRAPs consisting of amphiphile Brij L4. The thin nanosheets of ZIF-8 doped with Co^{2+} (Co-ZIF-8) synthesized by the same method maintained a high specific surface area after calcination. Therefore, the oxygen reduction reactions (ORR) activity of the calcined Co-ZIF-8 NSs for fuel cells becomes higher than calcined conventional Co-ZIF-8 crystals.

Introduction

Synthesis methods for functional nanosheets (NSs) have developed in terms of versatility. Since the first NSs were obtained from the exfoliation of a natural layered material, various NSs of layered materials have been fabricated by this top-down method.[1] The top-down preparation of graphene, one atom thick crystal with unique properties,[2] prominently promotes the development of the top-down method.[3] Meanwhile, to prepare NSs of non-layered materials, the bottom-up two-dimensional (2-D) growth with various templates has been explored. Chemical vapor deposition (CVD), in which the epitaxial growth occurs on a flat substrate, is one of the most studied hard template methods at the gas-solid interface.[4] Precursors are randomly supplied on the solid surface, and the resulting NSs are immobilized there. NSs preparation at the solid-liquid interfaces has the same characteristics.[5,6] The NSs preparation at liquid-liquid and gas-liquid interfaces gives rise to free-standing NSs without substrate removal process.[7,8] Since NSs are free to grow in the thickness direction toward the fluid phase, precursor supply must be well controlled to prepare thin and uniform NSs.

To produce high-quality NSs on a large scale, NSs preparation between layers of layered materials improves the growth inhibition in the thickness direction by restricting the space.[9] As another layered template, the lyotropic lamellar phase of amphiphilic solutions is also useful because the templates can be removed more easily than layered solids.[10] Bilayers in the lyotropic lamellar phases work as NSs generators for both hydrophilic and hydrophobic materials that can be obtained in

solution. Therefore, this method is promising as one of the most versatile preparation methods of NSs. Whereas materials tend to form thick NSs due to the high concentration of the ingredients and the close contacts between adjacent NSs in ordinary lamellar phases, separated bilayers in hyperswollen lyotropic lamellar (HL) phases inhibit such an NSs thickening process. Therefore, it looks suitable for the large-scale production of thin NSs of non-layered materials.[11]

The NSs preparation method using the HL phases is called 'two-dimensional reactors in amphiphilic phases (TRAP)' method.[11-14] The several nm thick two-dimensional (2-D) bilayers in the HL phases can one-dimensionally inhibit materials growth because they keep several hundred nm intervals between two adjacent bilayers.[15] TRAP method using HL phases of aqueous and organic amphiphile solutions can give hydrophobic and hydrophilic NSs, respectively; hydrophobic polystyrene NSs and hydrophilic gold NSs grow in the corresponding HL phase from single hydrophobic and hydrophilic precursors, respectively.[11,14] Moreover, metal-organic frameworks (MOFs) NSs as hydrophobic NSs can be synthesized from multiple precursors.[12,13] Unprecedented synthesis of hydrophilic NSs from multiple precursors should be tried to confirm the versatility of the TRAP method, as shown in Fig. 1.

We focused on zeolitic imidazolate frameworks (ZIFs) that are one kind of hydrophilic non-layered MOFs consisting of hydrophilic imidazole derivatives and metal ions. In particular, zinc 2-methylimidazolate with a sodalite-like framework (ZIF-8) is one of the most vigorously investigated ZIFs because it shows high separation performance,[16,17,18] adsorption capacity,[19] catalytic ability[20], water splitting[21,22], and energy storage[23-25] due to their porous structures. Oxygen reduction reaction (ORR) activity of the carbon electrocatalysts synthesized by calcining ZIF-8 doped with Co^{2+} (Co-ZIF-8) has recently been investigated to replace the present Pt/C.[26] The calcination of Co-ZIF-8 NSs is expected to give electrocatalysts with a larger specific surface

area than that of conventional Co-ZIF-8 crystals; it could be appropriate for ORR. Even the thinnest ZIF-8 NSs reported is about 30 nm.[27,28] Here we report the synthesis of several nm thick ZIF-8 NSs inside the hydrophilic TRAPs in a decane solution of amphiphile. We also discuss the synthesis condition that gives ZIF-8 selectively; zinc 2-methylimidazolate has two other frameworks: diamondoid (dia) and katsenite (kat).[29] We demonstrate the ORR activity of carbon electrocatalysts prepared by calcinating the obtained Co-ZIF-8 NSs and discuss it in terms of the multiscale porous structures.
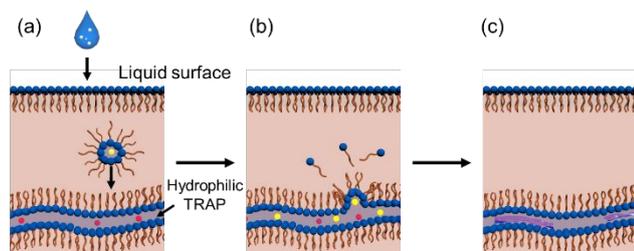
Fig.1 Schematic illustration of the mechanism of the precursor supply. (a) When the droplet of hydrophilic precursor solution is added to the hydrophilic TRAP solution, amphiphiles solubilize it as micelles. (b) The micelles marge with the hydrophilic bilayers of the HL phase. (c) Hydrophilic nanosheets grow inside the bilayers.

Experimental

Chemicals

Decane, 2-methylimidazole (2-mim), 25 wt% ammonium hydroxide solution, isopropanol, Nafion, zinc nitrate hexahydrate ($ZnNO_3 \cdot 6H_2O$) and cobalt nitrate hexahydrate ($CoNO_3 \cdot 6H_2O$) were purchased from Wako Pure Chemical Industries Co. Brij L4, Potassium hydroxide (KOH) and Pt/C (20% loading) was purchased from Merck KGaA. The water used was obtained from a water purifier (Direct-Q UV) with a resistivity of 18.2 MΩ cm.

Characterization

The crystal structures were estimated from XRD patterns collected using a PANalytical X'Pert PRO diffractometer with Cu Kα radiation, operated at 45 kV and 40 mA. The scan range was from 5º to 45º (2θ) at 0.10º/s. AFM images were obtained using a Veeco Instruments MMAFM-2. The samples were deposited on freshly exfoliated mica sheets as substrates. We measure 30 samples and calculated the average and standard deviation of the size and thickness, respectively. TEM images were obtained using a Hitachi H-800 at 200 kV. The distributions of ZIF-8 NSs were measured by DLS using ELSZ-2000 (Otsuka Electronics Co., Ltd.) at 25°C. FT-IR spectra were measured using a Shimazu IRAffinity-1S. The porosity of the products was characterized by Nitrogen adsorption measurements at 77 K using a BELSORPmax (MicrotracBEL). X-ray photoelectron spectroscopy (XPS) spectrum on C 1s and N 1s were obtained in a VG-Microtech Multilab 3000 spectrometer with an Al Kα radiation (1253.6 eV) as the energy source.

Synthesis of ZIF-8 NSs

ZIF-8 NSs were synthesized in the hyperswollen lyotropic lamellar (HL) phases of the decane solutions of Brij L4 (8.7 wt%) and deionized water (2.2 wt%). Ammonium hydroxide solution (25 wt%) and 2-methylimidazole (2-mim) were added to the decane solution at 1.1×10^{-1} wt% and 3.0×10^{-2} wt%, respectively. $Zn(NO_3)_2$ solution (14 wt%, 0.1 ml) was added to the decane solution (45 ml) so that the molar ratio of the Zn and 2-mim to the 1:2 at 39ºC. The final products were centrifuged at 11,000 rpm for 1 h and washed three times with methanol.

Synthesis of conventional ZIF-8 crystals

Conventional ZIF-8 crystals were synthesized in an aqueous Brij L4 solution consisted of deionized water (85.5 wt%) and Brij L4 (4.3 wt%). Ammonium hydroxide solution (25 wt%) and 2-methylimidazole (2-mim) were added to the decane solution at 2.9×10^{-1} wt% and 4.7 wt%, respectively. $Zn(NO_3)_2$ solution (19.7 wt%, 10 ml) was added to the aqueous Brij L4 solution (32 ml) so that the molar ratio of the Zn and 2-mim to the 1:2 at 39 ºC. The final products were centrifuged at 11,000 rpm for 1 h and washed three times with methanol.

Oxygen reduction reaction

Electrochemical activity tests towards ORR were carried out at 298 K in a three-electrode cell with 0.1 M KOH electrolytes using VersaSTAT3 Potentiostat (AMETEK), a Pt coil electrode as the counter electrode and a saturated calomel electrode as the reference electrode. A rotating ring-disk electrode setup (RRDE-3A, Pine Research Instruments, USA) equipped with a glassy carbon (GC) disk was used as the working electrode. The samples were dispersed in a solution of 10 vol% of isopropanol, 10 vol% of Nafion, and 80 vol% of water to prepare a final dispersion of 1 mg/ml of the prepared catalysts. And then, 4 µl of the dispersion was pipetted on a GC electrode to obtain uniform catalysts layer for ORR study. Cyclic Voltammetry (CV) and linear sweep voltammetry (LSV) from 1.2 to 0.2 V vs. RHE were carried out. The LSV was done in an O_2-saturated atmosphere at 1,600 rpm.

Results and discussion

The HL phases for the TRAP method have to be stable even in the addition of the precursors and reagents.[11] The decane solution of Brij L4 with a small amount of water has been reported to exhibit a promising HL phase with hydrophilic TRAPs.[14] The polarized photograph of the decane solution using a polarizing film wrapped around the vessel shows a birefringence typical of HL phases, as shown in Fig. 2a.[14] First, we dissolved ammonium hydroxide and 2-mim in the hydrophilic TRAP solution. It did not affect the stability of the HL phase, as shown in Fig 2b and 2c. The hydrophilic bilayers probably trapped 2-mim stably. Whereas the synthesis of ZIF-8 in an aqueous solution generally needs the excess amount of 2-methylimidazole (2-mim) relative to Zn^{2+} ion, ZIF-8 crystals grow in some aqueous amphiphile solutions even with those precursors at the stoichiometric ratio ([2-mim]/[Zn^{2+}] = 2) because the amphiphiles stabilize the coordination structure of ZIF-8.[30] Then, an aqueous $Zn(NO_3)_2$ solution was added to the

hydrophilic TRAP solution so that [2-mim]/[Zn^{2+}] would become 2.2. Phase separation occurred once immediately after adding $Zn(NO_3)_2$, and then, the mixture became homogeneous again, as shown in Fig. S1. The phase transition might be attributed to the tentative heterogeneity of Brij L4 concentration. Even after the rehomogenization, the TRAP solution still maintained the HL phase, as shown in Fig. 2d. These results suggest that the addition of precursors does not destabilize the HL phase.
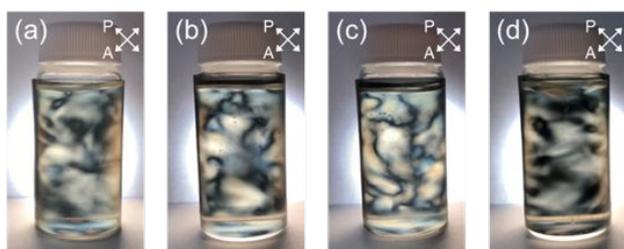
Fig. 2 Polarized photographs of a hyperswollen lyotropic lamellar phase of decane solution of Brij L4 (1.8×10^{-1} M), and water (1.0 M) with the following additives: (a)No additives, (b) ammonium hydroxide (1.2×10^{-2} M), (c) ammonium hydroxide (1.2×10^{-2} M) and 2-mim (2.8×10^{-3} M), and (d) ammonium hydroxide (1.2×10^{-2} M) and 2-mim (2.8×10^{-3} M) and $Zn(NO_3)_2$ (1.2×10^{-3} M).

After stirring the TRAP solution for 24 h, we centrifuged the reaction mixture at 11,000 rpm for 1 h, washed the obtained white powder with methanol three times, and dried it. The X-ray diffraction (XRD) pattern of the obtained powder shows the same peaks as conventional ZIF-8 crystals, as shown in Fig. 3a. The full width at half maximum (FWHM) of each of the XRD peaks for the obtained powder was broader than that of conventional ZIF-8 crystals, as shown in Table S1. The Williamson-Hall plots shown in Fig. S2 indicate that the crystallite size of the obtained powder is smaller than that of conventional ZIF-8 crystals.[31] The transmission electron microscopy (TEM) photograph shows sheet-like particles (Fig. 3b). The thickness and horizontal width of the particles measured by atomic force microscopy (AFM) are 1.5 ± 0.3 nm
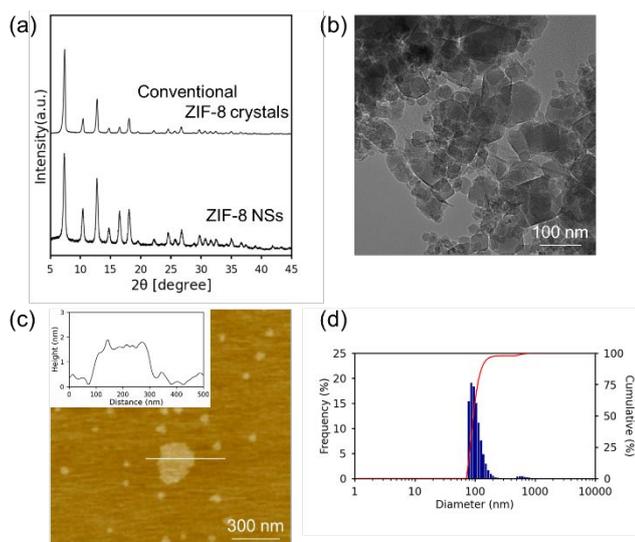
Fig. 3 Characterization of ZIF-8 NSs. (a) X-ray diffraction patterns of the ZIF-8 NSs, and conventional ZIF-8 crystals. (b) TEM photograph of ZIF-8 NSs. (c) AFM photograph and cross-section of one of the synthesized ZIF-8 NSs. (d) DLS analysis of ZIF-8 NSs.

and 125 ± 98 nm, respectively, as shown in Fig. 3c. The horizontal width could be controlled with constant thickness by the Reynolds number of the solution.[14] The particle size distributions estimated from dynamic light scattering (DLS) measurements of the aqueous dispersion of the powder suggest the absence of the aggregates, as shown in Fig. 3d. These results indicate that the obtained powder is ZIF-8 NSs and that Brij L4 plays a role in the nanosheet formation.

The nitrogen adsorption isotherm of the ZIF-8 NSs shows that the micropore volume of the ZIF-8 NSs is smaller than that of conventional ZIF-8 crystals, as shown in Fig. S3a. It indicates that the thinner the NSs are, the smaller the micropore volume because pore volume decreases as the external surface area increases relative to the volume. Besides, the gate-opening gas adsorption was not detected for the ZIF-8 NSs, as shown in Fig. S3b.[32] It is consistent with previous studies that reported the absence of structural transitions in ZIF-8 isotherms for nanosized particles.[33] Thus, although we confirmed that the internal surface area is alive without being filled, the role of Brij L4 in the formation of the ZIF-8 structure is still ambiguous.

We synthesized zinc 2-metylimidazolate in an aqueous Brij L4 solution with various concentrations to investigate the effect of Brij L4 on polymorphism. The ratios of $ZnNO_3$ and 2-mim to water are the same as those for ZIF-8 NSs synthesis; however, decane was not added to the solution. The XRD pattern of the product synthesized without Brij L4 has only the typical peaks of dia(Zn), as shown in Fig. S4a.[34] Another XRD pattern indicates the mixture of ZIF-8 and dia(Zn) was perhaps obtained even when the ratio of [Brij L4]/[Zn^{2+}] was 9.4×10^{-3} : 1, as shown Fig. S4b. These results suggest that the addition of Brij L4 induces the formation of ZIF-8. Further increasing the Brij L4 concentration, the pure conventional ZIF-8 crystals were produced. To check if Brij L4 stabilizes the coordination structure of ZIF-8, we performed the Fourier transform infrared spectroscopy (FT-IR). ZIF-8 NSs have peaks derived from methyl and methylene groups of Brij L4, as shown in Fig. S5. Brij L4 is adsorbed at the surface of the washed ZIF-8 NSs. These peaks are not derived from 2-mim, as shown in Fig. S5. We presume that conventional ZIF-8 crystals did not show these peaks because the external surface areas of conventional ZIF-8 crystals are smaller than those of the ZIF-8 NSs. Therefore, we can conclude that Brij L4 probably stabilizes ZIF-8.

To synthesize a high-performance ORR catalyst, we have to dope ZIF-8 NSs with Co^{2+} ions. We examine the stability of the HL phase when $Co(NO_3)_2$ is added in an aqueous solution of $Zn(NO_3)_2$. First, we dissolved ammonium hydroxide and 2-mim in the hydrophilic TRAP solution. Then, an aqueous $Zn(NO_3)_2$ solution dissolving a small amount of $Co(NO_3)_2$ was added to the hydrophilic TRAP solution so that [2-mim] : [Zn^{2+}] : [Co^{2+}] became 2.2 : 1 : 4.9×10^{-2}. After adding Zn^{2+} and Co^{2+}, the TRAP solution still maintained the HL phases, as shown in Fig. S6. Thus, the addition of $Co(NO_3)_2$ does not seem to destabilize the HL phase.

After stirring the TRAP solution for 24 h, we centrifuged the reaction mixture at 11,000 rpm for 1 h, washed the obtained purple powder with methanol three times, and dried it. The XRD pattern of the obtained powder shows the same peaks as
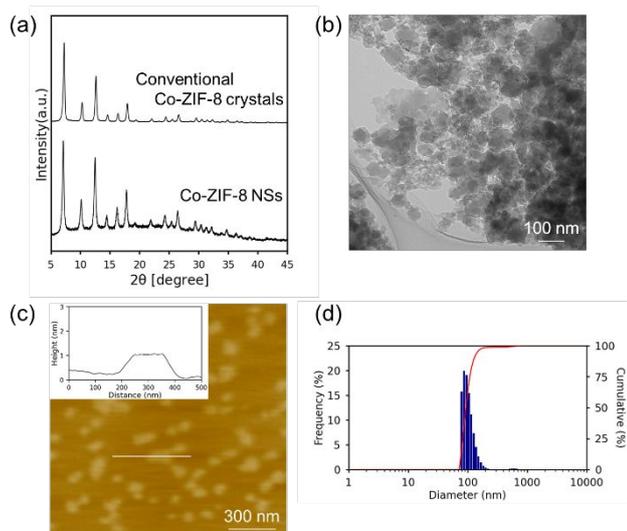
Fig. 4 Characterization of Co-ZIF-8 NSs. (a) X-ray diffraction patterns of the Co-ZIF-8 NSs, and conventional Co-ZIF-8 crystals. (b) TEM photograph of Co-ZIF-8 NSs. (c) AFM photograph and cross-section of one of the synthesized Co-ZIF-8 NSs. (d) DLS analysis of Co-ZIF-8 NSs.

Fig. 5 ORR activities of calcinated Co-ZIF-8 NSs, calcinated conventional Co-ZIF-8 crystals, and Pt/C 20 wt%.

conventional Co-ZIF-8 crystals, as shown in Fig.4a. The FWHM of each of the XRD peaks for the obtained powder was broader than that of conventional Co-ZIF-8 crystals, as shown in Table S2. The Williamson-Hall plots shown in Fig. S7 indicate that the crystallite size of the obtained powder is smaller than that of conventional Co-ZIF-8 crystals.[29] The TEM photograph shows sheet-like particles (Fig. 4b). The thickness and horizontal width of the particles measured by AFM are 0.9 ± 0.1 nm and 162 ± 40 nm, respectively, as shown in Fig. 4c. The particle size distributions estimated from DLS of the aqueous dispersion of the powder suggest the absence of the aggregates without any purification, as shown in Fig. 4d. These results indicate that the obtained powder is Co-ZIF-8 NSs. Nitrogen adsorption measurements show that the micropore volume of Co-ZIF-8 NSs is almost the same as the ZIF-8 NSs, as shown in Fig. S8a. Therefore, the obtained Co-ZIF-8 NSs seem appropriate for ORR.

We calcinated the Co-ZIF-8 NSs and measured ORR activity. After calcination of Co-ZIF-8 NSs at 800°C for 3 h under nitrogen atmosphere, we obtained carbon powder. The XRD pattern of the obtained powder does not show any peaks, as shown in Fig S9. It indicates that neither zinc nor cobalt crystalized as metals or compounds in the calcination. The TEM photographs indicate that the samples are aggregated after calcination; however, the structures partially remained, as shown in Fig. S10. The micropore volume of the conventional Co-ZIF-8 crystals decreased in the calcination because of the deformation of the porous structures, as shown in Fig. S8b. Meanwhile, the micropore volume of the calcinated Co-ZIF-8 NSs was almost the same as the precursor, as shown in Fig. S8a. Brij L4 adsorbed on the surface of Co-ZIF-8 NSs might stabilize the structure. We will briefly discuss it later. Accordingly, the surface area of Co-ZIF-8 NSs was larger than that of conventional ZIF-8 crystals, as shown in Table S3. The improved surface area of ZIF-8 NSs would have a positive influence on the ORR.
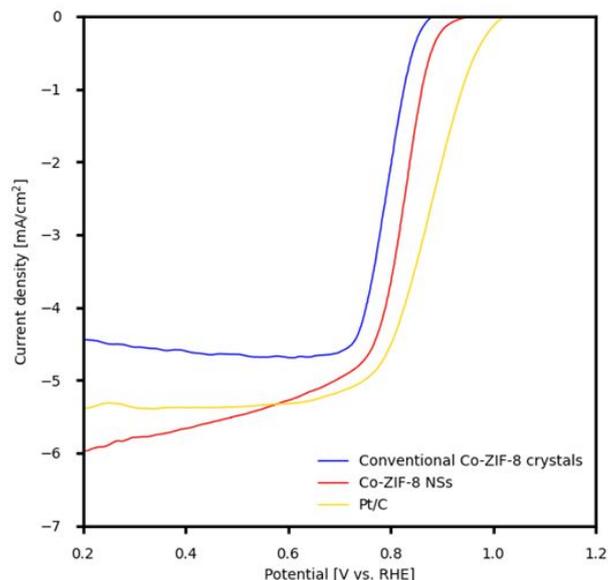
We measured the ORR activities of these calcinated ZIF-8 samples. The calcinated Co-ZIF-8 NSs show higher ORR activity than calcinated conventional Co-ZIF-8 crystals, as shown in Fig. 5. Limiting current density of calcinated Co-ZIF-8 NSs is better than that of calcinated conventional Co-ZIF-8 crystals and becomes better than that of Pt/C 20 wt% under the potential 0.5 vs. RHE. This result should come from the improvement of diffusivity. Moreover, the onset potential of calcinated Co-ZIF-8 NSs was also better than the calcinated conventional Co-ZIF-8. This result shows that the CoNx site of calcinated Co-ZIF-8 NSs has high catalytic activity. Therefore, we could conclude that the increase of the outer surface area promotes the ORR activity. Meanwhile, the onset potential did not reach 20% Pt/C. The XPS spectrum shows that the C-O peak and oxidized N peak of the calcinated Co-ZIF-8 NSs are higher than these of calcinated conventional Co-ZIF-8 crystal, as shown in Fig. S11. The oxygen atoms seem to be derived from Brij L4, and they might suppress the ORR activity. The calcinated ZIF-8 NSs would have higher activity if Brij L4 could be completely removed. Amphiphile not containing oxygen atom might solve this problem.

Conclusions

Several nm thick ZIF-8 NSs have been successfully synthesized from multiple hydrophilic precursors inside the hydrophilic TRAPs in a decane solution of amphiphile Brij L4. It is the first example of the preparation of hydrophilic nanosheets from multiple precursors using the TRAP method. The TRAP method looks like a versatile method for the large-scale production of thin NSs of various non-layered materials. On the one hand, Brij L4 stabilizes the coordination structure of ZIF-8, allowing the formation of pure ZIF-8 crystals in a solution of precursors with the stoichiometric ratio. On the other hand, Brij L4 perhaps inhibits the growth of the other frameworks: diamondoid and katsenite. Moreover, the Co-ZIF-8 NSs obtained by the same method maintained a high specific surface area after

calcination. We speculate that it is because Brij L4 adsorbed on the surface of Co-ZIF-8 NSs stabilize the framework during calcination. Because of the improved diffusivity, the calcinated Co-ZIF-8 NSs show higher ORR activity than the calcinated conventional Co-ZIF-8 crystals. However, oxygen atoms derived from Brij L4 are likely to suppress the ORR activity of the calcinated Co-ZIF-8 NSs. Amphiphiles containing fewer oxygen atoms might solve this problem.

Conflicts of interest

There are no conflicts to declare.

Acknowledgements

Notes and references

1   MacEwan, D. M. C.; Wilson, M. J. In Crystal Structures of Clay Minerals and Their X-ray Identification; Brindley, G. W., Brown, G., Eds.; Mineralogical Society of Great Britain and Ireland: Middlesex, United Kingdom, 1980, Chapter 3, p 197.
2   K. S. Novoselov, A. K. Geim, S. V. Morozov, D. Jiang, Y. Zhang, S. V. Dubonos, I. V. Grigorieva and A. A. Firsov, *Science*, 2004, **306**, 666–669.
3   F. I. Alzakia and S. C. Tan, *Adv. Sci.*, 2021, 2003864.
4   N.G. Shang, F.C.K. Au, X.M. Meng, C.S. Lee, I. Bello and S.T. Lee, *Chem. Phys. Lett.*, 2002, **358**, 187–191.
5   B. Jang, M. Park, O. B. Chae, S. Park, Y. Kim, S. M. Oh, Y. Piao and T. Hyeon, *J. Am. Chem. Soc.*, 2012, **134**, 15010–15015.
6   G. Zhao, J. Li, X. Ren, J. Hu, W. Hu and X. Wang, *RSC Adv.*, 2013, **3**, 12909–12914.
7   A. Sanyal and M. Sastry, *Chem. Commun.*, 2003, 1236–1237.
8   L. Zhang, Y. Shen, A. Xie, S. Li, B. Jin and Q. Zhang, *J. Phys. Chem. B,* 2006, **110**, 6615–6620.
9   A. Wang, F. Kang, Z. Huang, Z. Guo and X. Chuan, *Microporous Mesoporous Mater.*, 2008, **108**, 318–324.
10 M. Adachi, K. Nakagawa, K. Sago, Y. Murata and Y. Nishikawa, *Chem. Comm*, 2005, 2381–2383.
11 Y. Uchida, T. Nishizawa, T. Omiya, Y. Hirota and N. Nishiyama, *J. Am. Chem. Soc.,* 2016, **138**, 1103–1105.
12 T. Omiya, K. Sasaki, Y. Uchida and N. Nishiyama, *ACS Appl. Nano Mater.*, 2018, **1**, 3779–3784.
13 T. Omiya, K. Sasaki, Y. Uchida and N. Nishiyama, *Mol. Cryst. Liq. Cryst.*, Taylor & Francis, 2019, **684**, 1–6.
14 K. Sasaki, T. Okue, T. Nakai, Y. Uchida and N. Nishiyama, *Langmuir*, 2021, **37**, 5872–5877.
15 F. C. Larche, J. Appell, G. Porte, P. Bassereau and J. Marignan, *Phys. Rev. Lett.*, 1986, **56**, 1700–1703.
16 S. R. Venna and M. A. Carreon, *J. Am. Chem. Soc.*, 2010, **132**, 76–78.
17 Q. Song, S. K. Nataraj, M. V. Roussenova, J. C. Tan, D. J. Hughes, W. Li, P. Bourgoin, M. A. Alam, A. K. Cheetham, S. A. Al-Muhtasebd and E. Sivaniah, *Energy Environ. Sci.*, 2012, **5**, 8359–8369.
18 Y. Pan, T. Li, G. Lestari and Z. Lai, *J. Membr. Sci.*, 2012, **390–391**, 93–98.
19 J. McEwen, J.-D. Hayman and A. O. Yazaydin, *Chem. Phys.*, 2013, **412**, 72–76.
20 L. T. L. Nguyen, K. K. A. Le and N. T. S. Phan, *Chin. J. Catal.*, 2012, **33**, 688–696.
21 H. Song, N. Wang, H. Meng, Y. Han, J. Wu, J. Xu, Y. Xu, X. Zhang and T. Sun, *Dalton Trans.*, 2020, **49(31)**, 10816–10823.
22 L. Ye, Y. Zhang, L. Wang, L. Zhao and Y. Gong, *Dalton Trans.*, 2021, **50(21)**, 7256–7264.
23 T. Chen, L. Ma, B. Cheng, R. Chen, Y. Hu, G. Zhu, Y. Wang, J. Liang, Z. Tie, J. Liu and Z. Jin, *Nano Energy*, 2017, **38**, 239–248.
24 G. Zhu, T. Chen, L. Wang, L. Ma, Y. Hu, R. Chen, Y. Wang, C. Wang, W. Yan, Z. Tie, J. Liu and Z. Jina, *Energy Storage Mater.*, 2018, **14**, 246–252.
25 T. Chen, W. Kong, M. Fan, Z. Zhang, L. Wang, R. Chen, Y. Hu, J. Ma and Z. Jin, *J. Mater. Chem. A*, 2019, **7**, 20302–20309.
26 P. Yin, T. Yao, Y. Wu, L. Zheng, Y. Lin, W. Liu, H. Ju, J. Zhu, X. Hong, Z. Deng, G. Zhou, S. Wei and Y. Li, *Angew. Chem. Int. Ed.*, 2016, **55**, 10800–10805.
27 Y. Jiang, H. Liu, X. Tan, L. Guo, J. Zhang, S. Liu, Y. Guo, J. Zhang, H. Wang, W. Chu, *ACS Appl. Mater. Interfaces*, 2017, **9**, 25239–25249.
28 X. Wei, D. Xu, K. Ge, S. Qi and Y. Chen., *J. Inorg. Organomet. Polym. Mater.*, 2020, **30(10)**, 3862–3868.
29 A. D. Katsenis, A. Puškarić, V. Štrukil, C. Mottillo, P. A. Julien, K. Užarević, M.-H. Pham, T.-O. Do, S. A. J. Kimber, P. Lazić, O. Magdysyuk, R. E. Dinnebier, I. Halasz and T, Friščic, *Nat Commun.*, 2015, **6,** 6662.
30 X. Fan, W. Wang, W. Li, J. Zhou, B. Wang, J. Zheng and X. Li, *ACS Appl. Mater. Interfaces*, 2014, **6**, 14994–14999.
31 J. Madhavi, *SN Appl. Sci.*, 2019, **1**, 1509.
32 D. Fairen-Jimenez, S. A. Moggach, M. T. Wharmby, P. A. Wright, S. Parsons and T. Düren, *J. Am. Chem. Soc.*, 2011, **133**, 8900–8902.
33 C. Zhang, J. A. Gee, D. S. Sholl and R. P. Lively, *J. Phys. Chem. C*, 2014, **118**, 20727–20733.
34 Q. Shi, Z. Chen, Z. Song, J. Li and J. Dong, *Angew. Chem. Int. Ed.*, 2011, **50**, 672–675.